High-resolution monitoring of diffuse (sheet or interrill) erosion using structure-from-motion

Bernardo M. Cândido[a,b,*], John N. Quinton[a], Mike R. James[a], Marx L. N. Silva[b], Teotônio S. de Carvalho[b], Wellington de Lima[b], Adnane Beniaich[b], Anette Eltner[c]

[a]Lancaster Environment Centre, Lancaster University, Lancaster, UK

[b]Soil Science Department, Universidade Federal de Lavras, Lavras, Brazil

[c]Institute of Photogrammetry and Remote Sensing, Technische Universität Dresden, Dresden, Germany

*Corresponding author

E-mail addresses: bernardocandido@gmail.com (B.M. Cândido), j.quinton@lancaster.ac.uk (J.N. Quinton), m.james@lancaster.ac.uk (M.R. James), marx@ufla.br (M.L.N. Silva), teotonio.carvalho@ufla.br (T.S. de Carvalho), anette.eltner@tu-dresden.de (A. Eltner).

Abstract

Sheet erosion is common on agricultural lands, and understanding the dynamics of the erosive process as well as the quantification of soil loss is important for both soil scientists and managers. However, measuring rates of soil loss from sheet erosion has proved difficult due to requiring the detection of relatively small surface changes over extended areas. Consequently, such measurements have relied on the use of erosion plots, which have limited spatial coverage and have high operating costs. For measuring the larger erosion rates characteristic of rill and gully erosion, structure-from-motion (SfM) photogrammetry has been demonstrated to be a valuable tool. Here, we demonstrate the first direct validation of UAV-SfM measurements of sheet erosion using sediment collection data collected from erosion plots.

Three erosion plots (12 m × 4 m) located at Lavras, Brazil, with bare soil exposed to natural rainfall from which event sediment and runoff was monitored, were mapped during two hydrological years (2016 and 2017), using a UAV equipped with a RGB camera. DEMs of difference (DoD) were calculated to detect spatial changes in the soil surface topography over time and to quantify the volumes of sediments lost or gained. Precision maps were generated to enable precision estimates for both DEMs to be propagated into the DoD as spatially variable vertical uncertainties.

The point clouds generated from SfM gave mean errors of ~2.4 mm horizontally (*xy*) and ~1.9 mm vertically (*z*) on control and independent check points, and the level of detection (LoD) along the plots ranged from 1.4 mm to 7.4 mm. The soil loss values obtained by SfM were significantly ($p<0.001$) correlated (r^2 = 95.55%) with those derived from the sediment collection. These results open up the possibility to use SfM for erosion studies where channelized erosion is not the principal mechanism, offering a cost-effective method for gaining new insights into sheet, and interrill, erosion processes.

Key words: structure-from-motion, sheet erosion, UAV, photogrammetry, erosion plot, DEM of difference

1. Introduction

Soil erosion is one of the main factors that lead to the degradation of agricultural land worldwide (Boardman et al., 2003; Bakker et al., 2004; Zhao et al., 2019). It threatens agricultural sustainability by reducing the water retention capacity, the nutrient content, and total organic carbon of the soil (Quinton et al., 2010; Zhao et al., 2016), and it causes pollution of water bodies (Lal, 1998). Thus, the accurate measurement of erosion rates becomes a key factor for better understanding the erosive process in different scenarios and to promote efficient recovery strategies aiming to reduce soil loss in sloping areas (Cerdan et al., 2010; Di Stefano and Ferro, 2017).

Water flowing on a soil surface can be either dispersed or concentrated. Concentrated overland flow typically results in the formation of small channels, rills and gullies, while dispersed flow produces erosion which is diffuse and which leaves little trace after an erosion event (Al-Hamdan et al., 2012; Nouwakpo et al., 2016; Hernandez et al., 2017). Diffuse erosion is a complex mixture of shallow non-incised concentrated flows and areas of dispersed flow. In the literature it is referred to as sheet or interrill erosion; neither term is satisfactory. We prefer the term 'diffuse erosion', which we will use for the remainder of the paper, since erosion resulting from diffuse overland flow does not occur in sheets, nor does it always occur between rills.

The measurement of diffuse erosion provides a particular challenge: diffuse overland flow is difficult to monitor in the field due to its shallow depth and distributed nature. Radionuclides and sediment fingerprinting approaches can be used to differentiate diffuse erosion from rill and tillage erosion (Baumgart et al., 2017), but it is a time-consuming process, and topographic survey using GPS or total stations struggle to capture changes in surface elevation with sufficient spatial resolution (Parsons, 2019).

Diffuse erosion removes fine particles from the soil surface and, although not able to transport sediment over long distances, it is important in transporting sediment to rills and gullies (Evans et al., 2016; Parsons, 2019). Erosion plots provide the best means of determining erosion due to diffuse flow during natural and artificial rainfall conditions, when combined with observations of developed erosion forms on the plot. However, acquiring soil erosion data from erosion plots is time-consuming and costly (Cerdan et al., 2010), and limitations in spatial scale and restrictions for plot locations make this approach unsuited to large scale monitoring.

Digital elevation models (DEM) produced from high-resolution surveying techniques have played an important role in the understanding of geomorphological processes. These advances have been facilitated by the development of Structure-from-Motion (SfM; Ullman, 1979), a technique that combines well-established photogrammetric principles with modern computational methods (James and Robson, 2012). SfM photogrammetry, using images acquired from unmanned aerial vehicle (UAV), is being widely adopted for producing high-resolution DEMs in studies of surface processes (Colomina and Molina, 2014). The use of UAVs has made the acquisition of aerial photographs affordable and straightforward, allowing surveys at high temporal and spatial resolution. This makes it possible to monitor and quantify rapidly changing landscapes (Cook, 2017). In geosciences, the application of photogrammetry using SfM is now considered an established method to describe high-resolution topography (Cook, 2017; Eltner et al., 2018). This technique has been used in many Earth surface surveys, in studies of fluvial, glacial, and coastal geomorphological processes (Dietrich, 2016; Westoby et al., 2016; Warrick et al., 2017), as well as in the monitoring and quantification of gully erosion (Castillo et al., 2012; Gómez- Gutiérrez et al., 2014; Stöcker et al., 2015, Glendell et al., 2017). In addition, the use of UAVs and SfM photogrammetry has also been shown to be capable of evaluating of rill and interrill erosion (Bazzoffi, 2015; Eltner et al., 2015; Di Stefano et al., 2019; Kuo et al., 2019) although not verified against measured diffuse erosion rates.

However, UAV-based SfM-photogrammetry applications for studies of soil erosion where there are no large mass movements or gullies are still scarce. One study that has attempted to investigate diffuse erosion using UAVs is Pineux et al. (2017), who determined elevation changes for a small catchment in Belgium (124 ha), but did not compare their measurements against directly-measured volume-loss data. Over such areas, the image scales typically acquired (e.g. ground sampling distances of >5 cm) and the difficulties in defining a sufficiently precise and stable coordinate reference system, mean that quantifying the small magnitude changes that are typical of laminar erosion processes using UAVs is still challenging.

Assessment of the accuracy of data derived from SfM has been carried out by multiple studies (James and Robson, 2012; Westoby et al., 2012; Gómez-Gutiérrez et al., 2014; Eltner et al., 2015; Cook et al., 2017; James et al., 2017a; Morgan et al., 2017) using aerial and terrestrial laser scanning or control points with high precision as a reference. The reported accuracies vary widely from sub-decimetre to more than 1 m, reflecting the dependence of SfM accuracy on the image quality, distortion and orientation, vegetation presence, soil surface characteristics, number and precision of the ground control points and image scale. For good quality surveys, the relative precision ratio (measurement precision : observation distance) should exceed 1:1000, which implies centimetric precision over distances of 10s of metres (James and Robson, 2012).

Repeated topographic surveys of the same area are often carried out in order to establish spatial patterns of erosion, deposition, and changes in volume. Therefore, when successive DEMs are subtracted from each other, a DEM of difference (DoD) can be generated, allowing computations of the volume of soil lost or gained to be made (Lane et al., 2003). However, such volume measurements from UAVs, SfM and DoD have not been directly validated using measurements of sediment collected in standard erosion plots. The effectiveness of SfM for estimating diffuse erosion under artificial rain has been demonstrated by comparison with collected sediments in micro-scale laboratory plots (Balaguer-Puig et al. 2018); however, we are unaware of studies that validate the UAV-SfM approach with collected sediments under natural rainfall conditions. This leaves the question as to whether UAV-SfM can be used to obtain reliable soil loss measurements where channelized erosion is not the principal mechanism unanswered.

We answer this by demonstrating the first use of UAV-SfM to determine diffuse erosion that has been evaluated independently using sediment collection, allowing the study of the spatial distribution of laminar erosion processes along the plots, and its evolution over the time.

2. Materials and Methods

2.1. Experimental area

All the experiments were conducted on the campus of the Federal University of Lavras, Lavras, Brazil (21º13'20'' S and 44º58'17'' W), during two hydrological years. The area presents a typical humid subtropical climate, with an annual average rainfall of 1,530 mm. The soil is classified as an Inceptisol, according to Soil Taxonomy (Soil Survey Staff, 1999), with 47.8% sand, 15.8% silt and 36.4% clay, presenting a density of 1,400 kg m^{-3}. Three plots (12 m × 4 m) were installed in the area to monitor soil erosion on a 23% slope, under bare soil and natural rainfall conditions (Figure 1). The longest dimension of the plot followed the direction of the slope.

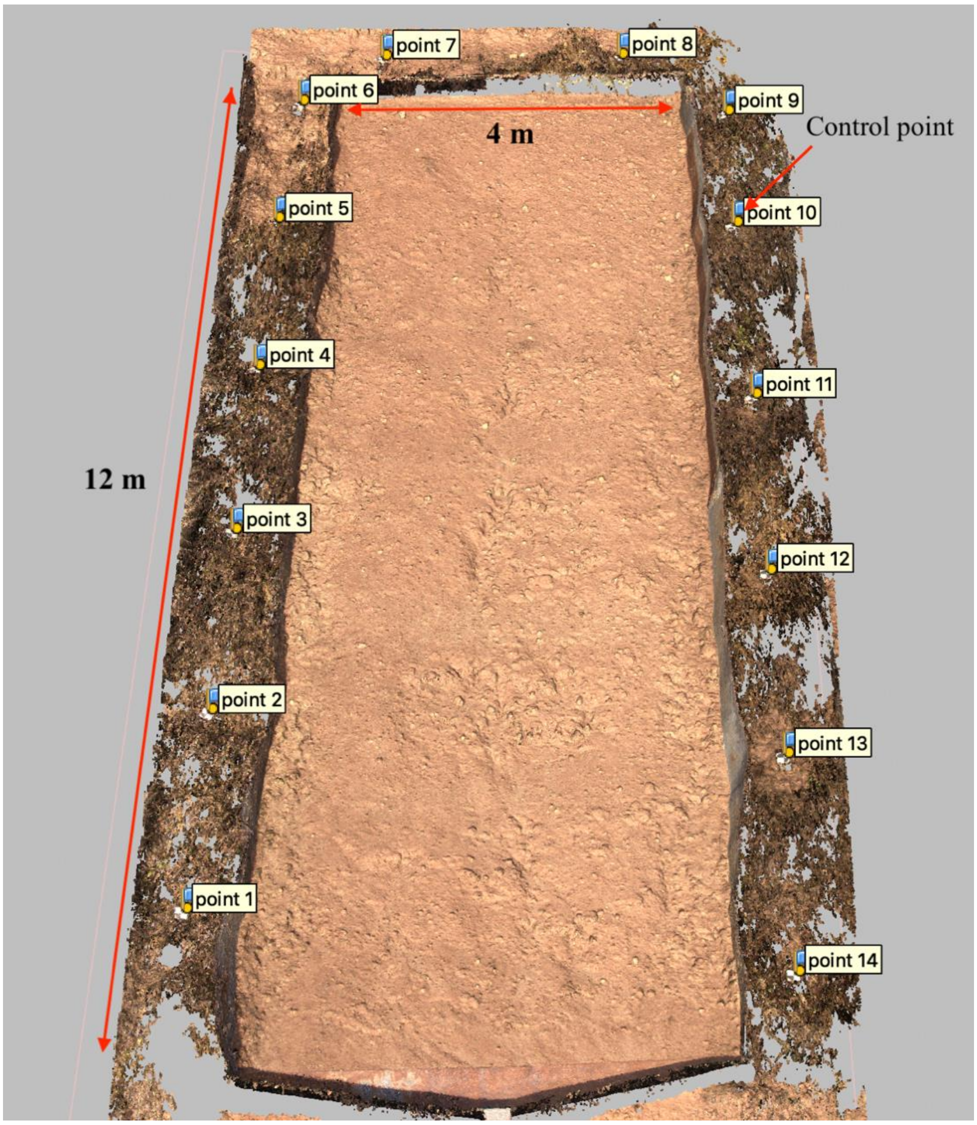

FIGURE 1 Typical erosion plot showing dimensions and control point layout.

2.2. Sediments measurements on erosion plots

The collector system comprised two tanks installed in sequence, the first with 500 L capacity and the second 250 L (Figure 2). Between the sedimentation tanks there was a Geib divisor system with 15 windows so that after filling the first tank, only 1/15 of the runoff was conducted to the second tank.

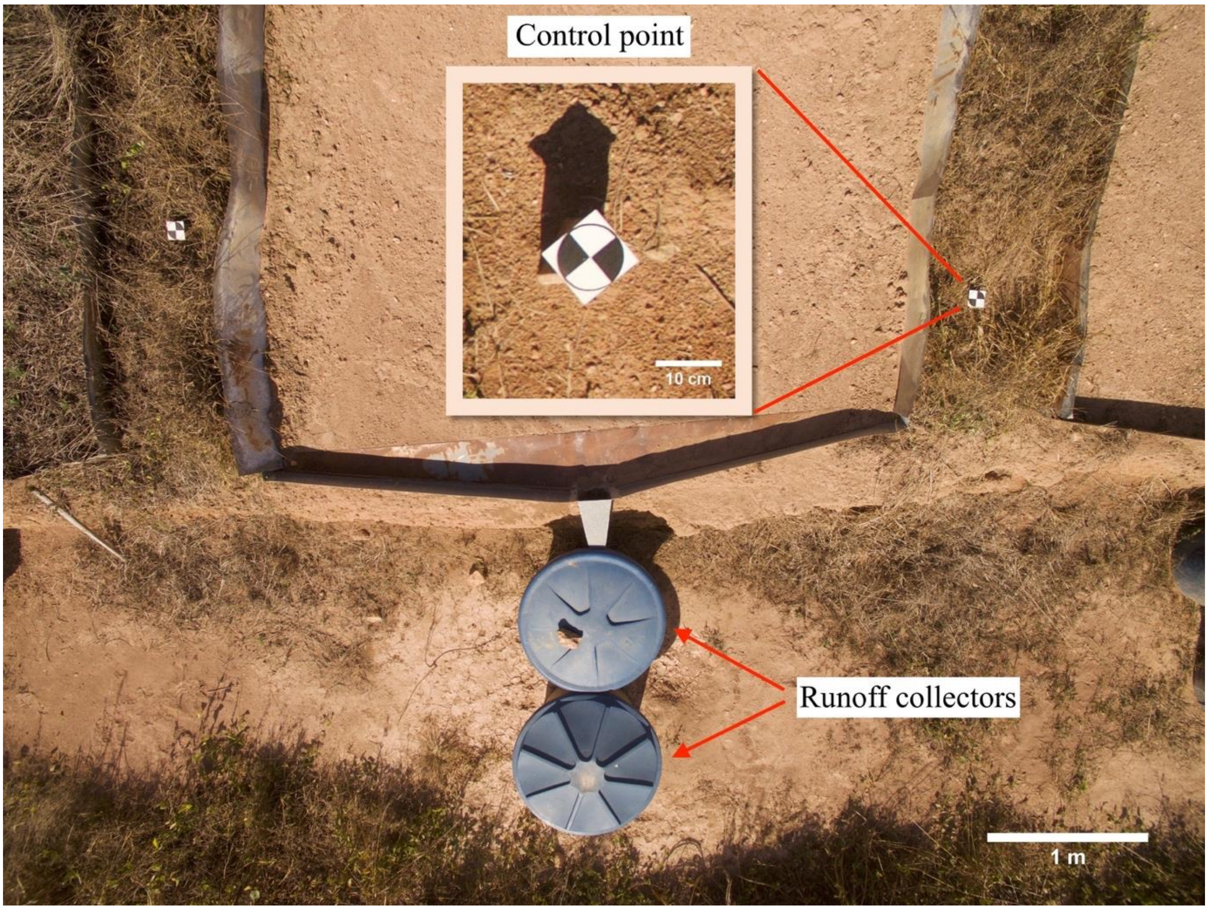

FIGURE 2 Runoff collection system used on soil loss plots. Inset shows the detail of a ground control point.

To quantify soil losses, runoff samples and sediments were collected from the collection tanks. After stirring, three aliquots of predetermined volume were collected, transferred to the laboratory, the supernatant decanted and the remaining sediment dried at 105°C before weighing.

2.3. Image acquisition

A DJI Phantom 3 Professional UAV was used for data acquisition. The UAV features an integrated gimbal-stabilized FC300X camera with 12-megapixel (4000 × 3000) Sony EXMOR 1/2.3 sensor, 94º field of view (FOV) and 20-mm focal length. The lens aperture was set to f/2.8 and images were acquired in RAW format.

Seven flights were performed on each erosion plot, from June 2016 to April 2018. The flights were conducted manually using a combination of orthogonal and oblique photos to provide convergent image geometries between the lines (James et al., 2014). In order to reduce the influence of direct sunlight at noon, flights were conducted either in the morning or in the afternoon on cloudy days. Flight heights were over 4 m with a nominal ground sampling distance of 1.5 mm. A total of 35 photos were taken in each survey, with 70% of forward and side overlap.

For georeferencing, 14 ground control points (GCP) were installed around the plots (Figure 1), with ten points used for control and four as check points to estimate the precision and the accuracy of the 3D models by calculating the root mean square error (RMSE). The coordinates of the points were established by total station (Geodetic GD2i, accuracy 2 mm), within an arbitrary local coordinate system.

2.4. Structure from motion (SfM) point cloud generation

The generation of three-dimensional point clouds (3D) was performed using the SfM photogrammetry technique, which allows the reconstruction of the topography from randomly distributed and oriented images from uncalibrated cameras (James and Robson, 2012; Fonstad et al., 2013; Agüera-Vega et al. 2018). The images were processed using the commercially available SfM software Agisoft Photoscan Professional® v1.4. All processing was done through cloud computing using a virtual machine (24 Intel Xeon Platinum 3.7 GHz CPUs, two NVIDIA Tesla K80 GPUs and 128 GB RAM).

Firstly, image alignment was done matching homologous image points across overlapping images. The next step calculates camera position and 3D location (*X*, *Y* and *Z*) of these tie points by means of a bundle-adjustment algorithm. For geo-referencing, ten control points were used in the bundle adjustment 'optimization' in Photoscan. This process further reduces non-linear distortions and minimises the total residual error on image observations by simultaneously adjusting camera parameters and orientations, and the 3D point positions. As a result of these first two steps, a sparse 3D point cloud was generated. The third step uses the camera information estimated previously, to produce a dense point cloud using multi-view stereo reconstruction. The dense point clouds were exported into Surfer® 16 software, converted to raster DEMs of 4-mm grid size using the nearest neighbour interpolation method, and cropped to remove the plot edges. The photogrammetric processing settings applied in Photoscan are listed in Table 1.

TABLE 1 Photoscan parameters settings used during the point cloud generation.

Point cloud: alignment parameters	Setting
Accuracy	Highest
Generic preselection	Yes
Reference preselection	Yes
Key point limit	120,000
Tie point limit	0
Filter point by mask	No
Dense point cloud: reconstruction parameters	
Quality	Medium
Depth filtering	Mild

2.5. Erosion measurements using SfM

The erosion calculations for each plot were performed using the Simpson's rule method (see Easa, 1988), which assumes nonlinearity in the profile between grid points. This technique shows greater precision in the determination of volume compared to linear methods, such as the trapezoidal rule (Fawzy, 2015). The soil volume was converted to mass (kg) by considering the soil bulk density, to correlate with the sediment collected from each runoff tank in the interval between the two drone flights.

DEMs of difference (DoD) were calculated to detect changes in the soil surface topography over time and to spatially quantify the volumes of sediment that were eroded and deposited. This technique consists of subtracting georeferenced DEMs from different periods to generate a raster of morphological (i.e. height) change:

$$\mathrm{DoD} = \mathrm{DEM}_{t2} - \mathrm{DEM}_{t1} \quad (1)$$

where *t1* is the initial time and *t2* is the consecutive time of DEM acquisition. Positive and negative values in the DoDs show deposition and erosion respectively.

2.6. DEM uncertainty and Level of Detection (LoD)

DEM uncertainty was assessed through the generation of precision estimates based on a Monte Carlo approach (James et al., 2017a), with post-processing tools in sfm_georef software (James and Robson, 2012). This method consists of repeated bundle adjustments in Photoscan, in which different pseudo-random offsets are applied to the image observations and to the control measurements to simulate observation measurement precision. Precision estimates for each optimised model parameter were then derived by characterising the variance for each particular parameter in the outputs from the large number of adjustments. In this study, 4,000 bundle adjustments were carried out, as used by James et al. (2017a).

Precision maps were generated through interpolation (4-mm grid size) of the vertical standard deviation (σ_Z) derived by the precision estimates, to enable precision estimates for both DEMs to be propagated into the DoD as spatially variable vertical uncertainties (Taylor, 1997; Wheaton et al., 2010). A 'level of detection' (LoD) of significant elevation change was calculated for each DoD cell, according to the equation:

$$\mathrm{LoD} = t(\sigma_{Z1}{}^2 + \sigma_{Z2}{}^2)^{1/2} \qquad (2)$$

where σ_{Z1} and σ_{Z2} are the vertical precision estimates for each cell in the two DEMs and t is the t-distribution value defined by a specific confidence level (this study 95%, giving t = 1.96). Thus, changes smaller than the LoD can be disregarded, and Surfer was used to generate the LoD-thresholded DoD maps.

2.7. Statistical analysis

For assessing the correlation between mass measurements obtained from sediment collection (M_{SC}) and from SfM (M_{SfM}) a linear regression model was fitted to the data. Because the same plots were repeatedly used through time for data collection, we investigated whether measurements from the same plot were statistically dependent by introducing a random intercept for each plot in the linear regression model, following a mixed modelling approach (Gelman and Hill, 2007; Zuur et al., 2009).

However, after fitting the model, we observed that the variance associated with the random intercept was null, indicating no evidence of statistical dependence caused by the plot effect. A drawback of that approach is the low number (three) of groups available for estimating the variance associated with the random effect of plots.

As an alternative approach to further investigate whether a statistical dependence among observations could be attributed to a plot effect, an analysis of covariance was performed, with both plot and SfM as explanatory variables, and amount of collected sediments as response variable. In agreement with the results from the previous approach, no significant effect of plots was observed ($F_{2,14} = 0.4$, $P = 0.68$). For the above reasons, the final model was simplified by omitting the plot effect and an ordinary linear regression approach was used, assuming statistical independence of the model residuals.

3. Results

3.1. Precision results

The photogrammetric errors (RMSE) calculated by the Photoscan on x,y and z-axes for the control, check and tie points of each SfM point cloud are listed in Table 2. The results show average errors of order ~2.2 mm in *x*, *y* and *z* on control (n=10) and check (n=4) points, and the tie points image residual RMS was ~ 0.3 pix.

TABLE 2 Root mean square error (RMSE) of check points, control points and tie points image residuals.

Plot	Date	RMS tie points image residuals (pix)	RMSE of control points (mm)	RMSE of check points (mm)

			X	Y	Z	X	Y	Z
	06/06/16	0.26	2.46	2.99	2.15	2.39	3.69	1.20
	22/08/16	0.24	2.16	1.63	1.90	1.14	1.58	2.69
	30/11/16	0.31	2.11	2.97	1.07	1.25	2.69	1.21
1	22/02/17	0.30	1.57	1.45	2.48	2.10	1.61	4.85
	25/05/17	0.32	2.74	3.52	1.64	1.38	3.31	2.33
	28/09/17	0.27	2.76	2.43	1.54	2.61	2.74	1.47
	26/04/18	0.29	1.17	0.80	0.57	1.02	1.13	1.95
	06/06/16	0.31	3.68	2.51	2.14	2.25	3.22	3.21
	22/08/16	0.29	3.75	1.83	1.12	3.33	2.26	2.77
	30/11/16	0.27	3.05	1.70	1.52	3.47	1.31	3.18
2	22/02/17	0.28	2.86	1.91	2.30	2.91	2.43	1.80
	25/05/17	0.32	3.75	2.18	2.55	1.01	1.17	1.86
	28/09/17	0.26	2.72	1.54	1.10	2.31	1.44	2.83
	26/04/18	0.39	2.42	2.01	2.27	3.08	2.07	1.83
	06/06/16	0.36	3.51	2.02	1.96	3.02	3.80	5.50
	22/08/16	0.33	3.13	2.70	1.28	3.51	1.71	0.74
	30/11/16	0.28	3.07	3.56	1.26	3.44	3.83	1.40
3	22/02/17	0.27	2.50	2.60	1.24	1.98	2.22	2.22
	25/05/17	0.33	1.72	2.19	1.00	0.94	2.30	2.66
	28/09/17	0.27	2.88	1.58	1.38	2.78	2.27	1.14
	26/04/18	0.29	1.54	2.28	1.17	1.46	2.70	1.65

The LoD maps show the spatial variation of precision along the plot (Figure 3), with values ranging from 1.4 mm to 7.4 mm. The larger values were concentrated in areas of less image overlap.

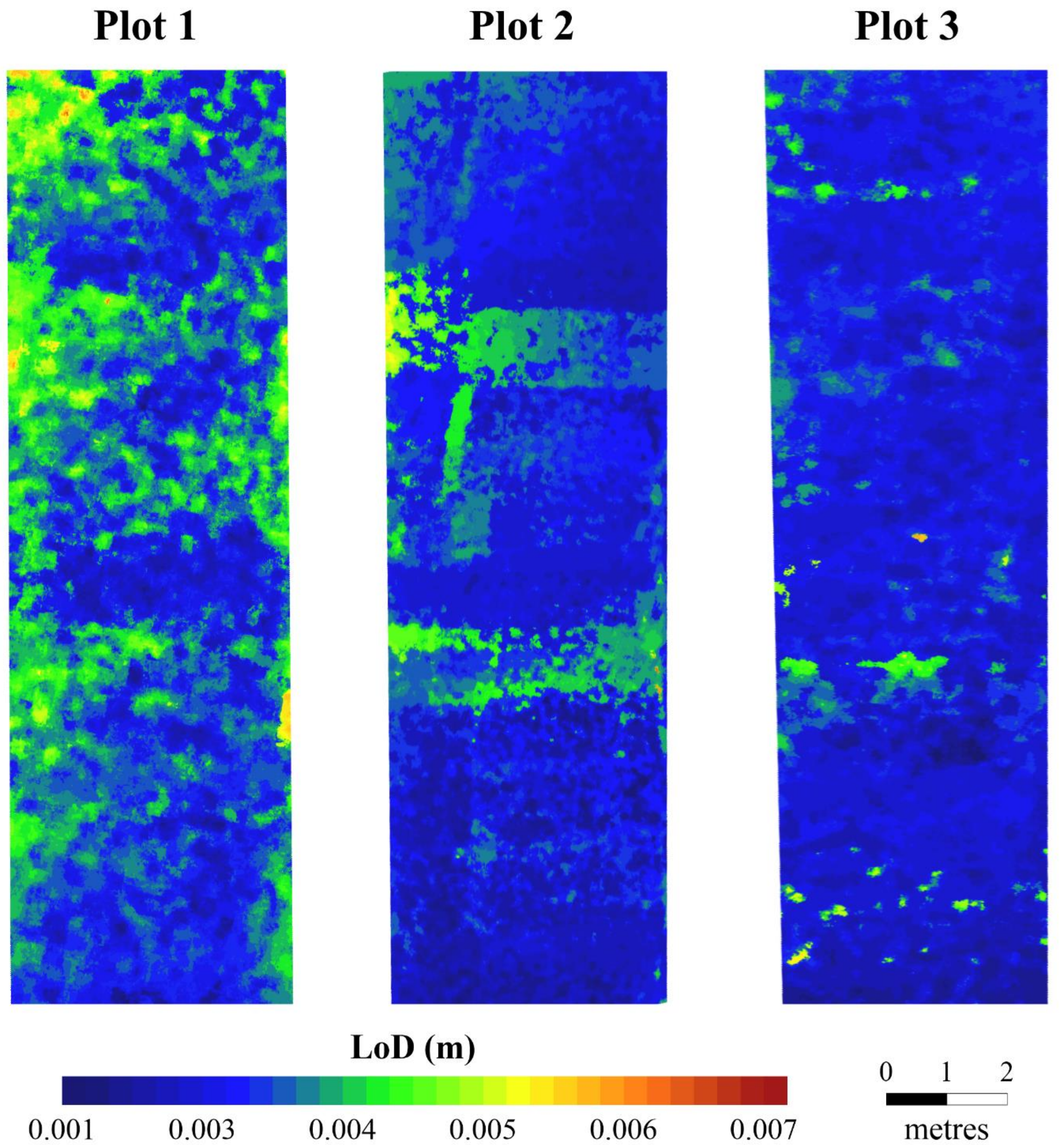

FIGURE 3 Level of detection (LoD) maps showing the spatial distribution of potential error along the plot. Changes with magnitudes smaller than the LoD can be disregarded.

3.2. DEM of Difference (DoD)

The DoD maps obtained from the erosion plots (Figure 4) showed remarkable variations in relation to soil movement over the studied period. Although erosion was predominant, it was also possible to detect soil deposition, mainly in the lower part of the plots near the sediment collectors. The periods where there were major soil movements were between November 2016 - February 2017 and September 2017 - April 2018 (Figures 4c and 4f), which match with the rainy season in the Southwest of Brazil. During the dry season, which corresponds to the period between May and September, less soil movement along the plot was visible in the DoD maps (Figure 4e).

Diffuse erosion was the predominant type of soil erosion over the study period. However, between September 2017 - April 2018, it was possible to observe the formation of rill erosion, where the highest rates of water erosion were concentrated.

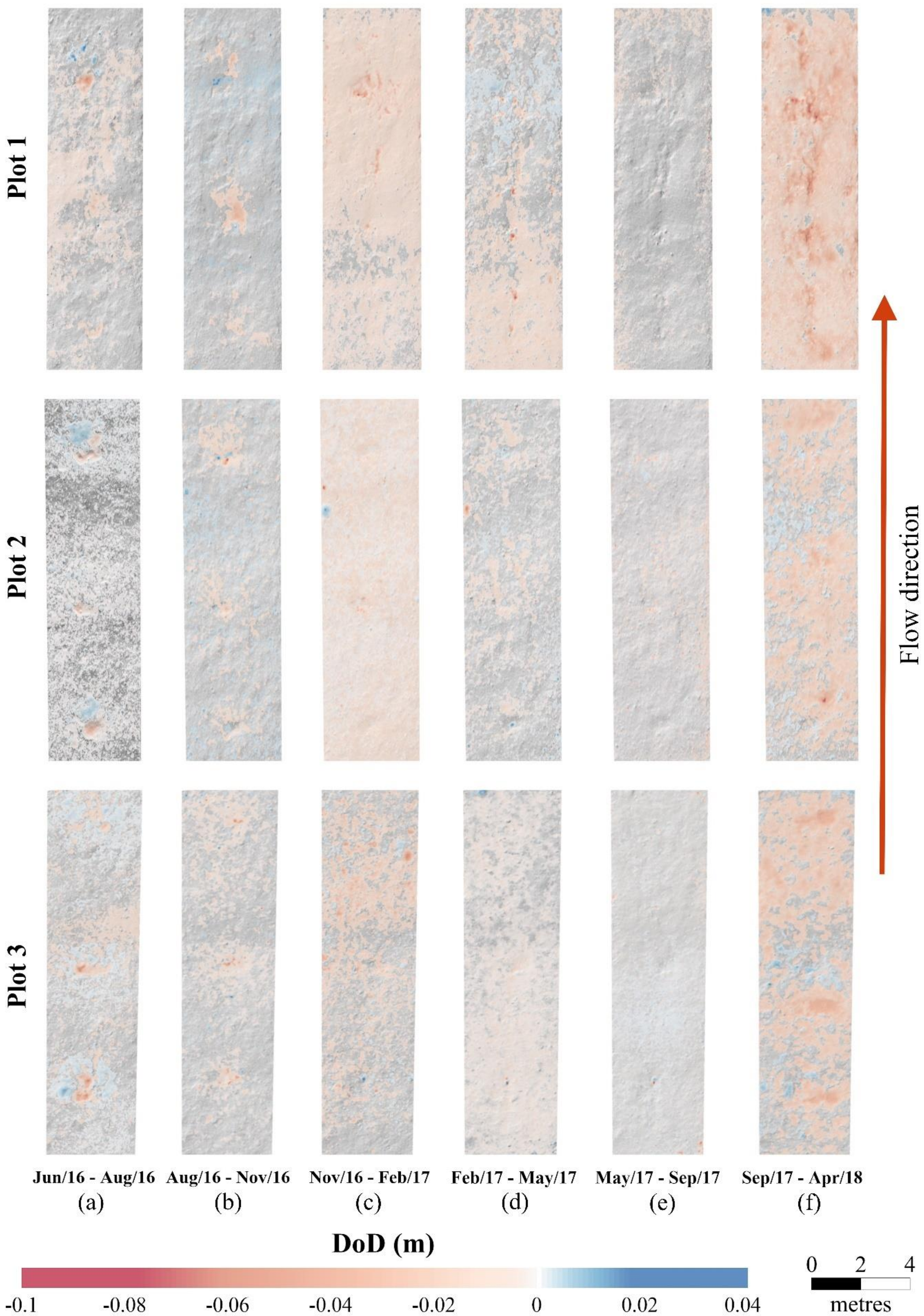

FIGURE 4 DEM of difference (DoD) maps, overlain over hillshaded topography, showing soil erosion over natural runoff. Colour scale ranges from red (erosion) to

blue (deposition). Transparent regions mean no significant changes (i.e. the DoD is less than the level of detection).

3.3. Erosion measurements

The soil loss values obtained by SfM showed a high correlation (R^2 = 95.55%) with the traditional sediment collection method (Figure 5). Values of soil losses obtained through the sediment collection tended to be slightly higher than those found by the SfM (Table 3). Soil loss measurements made by the SfM were closely related to the amount of sediments collected in all seasons of the year, both in summer (rainy season) and winter (dry season).

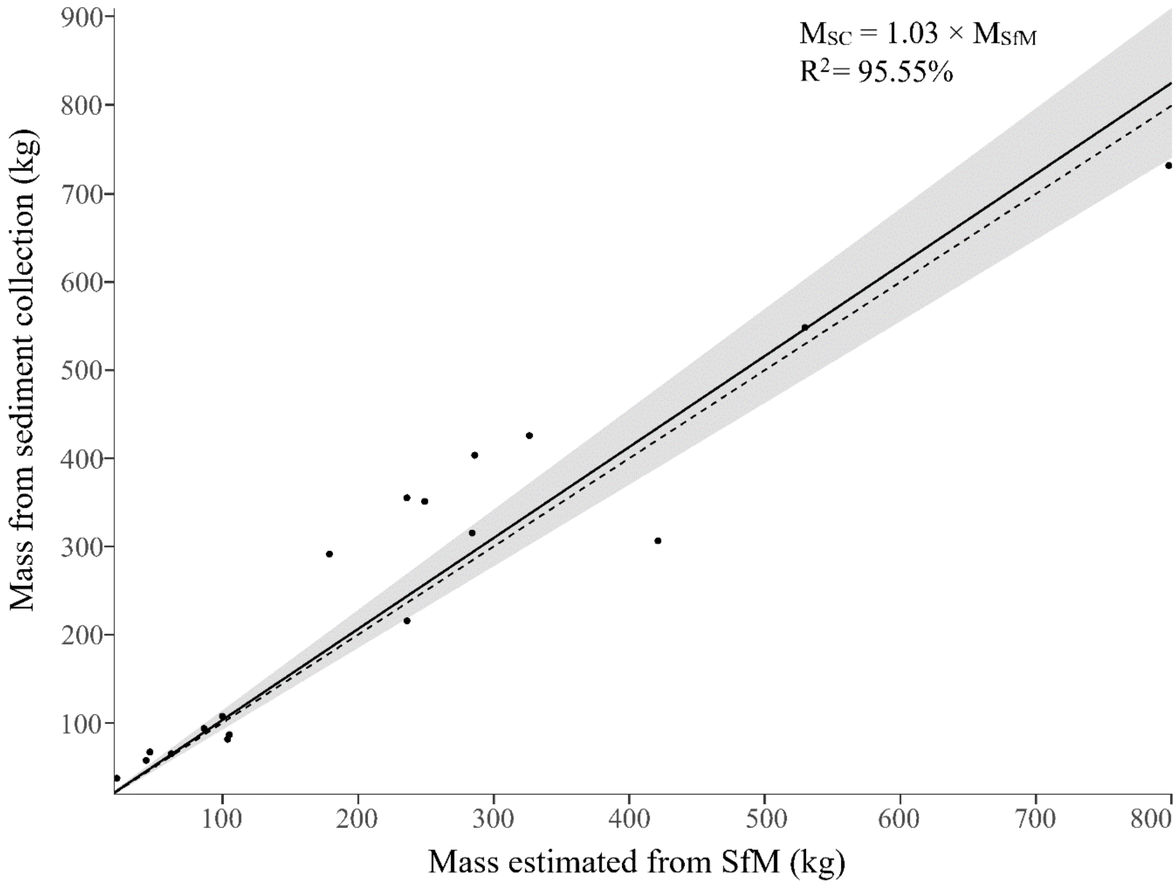

FIGURE 5 The relationship between the soil loss from sediment collection (M_{SC}) and

estimated from SfM (M_{SfM}). The dashed line represents the 1:1 relation. The grey zone is the confidence interval for the mean.

TABLE 3 Averaged soil loss calculated from sediment collection and structure from motion (SfM), and natural rainfall rates during each studied period.

Date	Sediments (kg)	SfM (kg)	Rainfall (mm)
Jun/2016 – Aug/2016	53.04	42.57	92
Aug/2016 – Nov/2016	129.93	127.40	194
Nov/2016 – Feb/2017	418.20	338.20	661
Feb/2017 – May/2017	304.33	294.67	149
May/2017 – Sep/2017	87.13	98.33	115
Sep/2017 – Apr/2018	520.45	470.11	1121

4. Discussion

4.1. Diffuse erosion measurements from UAV-SfM

This was the first time that UAV-SfM-based measurements of ‘diffuse erosion’ from natural rainfall have been evaluated independently using sediment collection as reference. The strong correlation between the soil loss from SfM and that collected in runoff tanks opens up the possibility to use UAV-SfM for erosion studies where channelized erosion is not the principal mechanism. For diffuse and sheet erosion of micro-scale laboratory plots exposed to simulated rain, Balaguer-Puig et al. (2018), obtained similar results. However, their SfM-based soil loss values slightly exceeded their measurements of collected sediments, which was not observed in this work (Table 3).

Our results represent a great step forward for soil erosion assessment as they offer the possibility of avoiding the limitations related to erosion plots, such as high operational costs, measurement variability due to human disturbance in collecting data (Zobisch et al., 1996) and the use of plots of different sizes (Bagarello and Ferro, 2004).Therefore, UAV-SfM can potentially increase the quality of the global soil erosion database.

Through UAV-SfM, it is possible to generate erosion and deposition maps that allow the volume of soil moved at different times and positions to be determined (Figure 4). Pineux et al. (2017) could detect diffuse erosion patterns at the watershed scale with UAV-SfM, but there were no independent field measurements to validate the technique. In addition, this method can distinguish the differences between soil eroded volume and soil lost volume. Also, it can be used to investigate the sediment delivery rate (Guo et al., 2016). In contrast, sediment and surface runoff collections are restricted to the evaluation of the amount of soil lost from the end of the monitored plot and give no information on the internal patterns of erosion and deposition nor the forms of erosion occurring on the plot.

However, SfM does rely on images of the soil surface, meaning that it is not suitable for areas with significant vegetation cover. SfM will also capture changes to the soil surface that are not due to erosion, for example the consolidation of the soil following tillage (Eltner et al., 2015), swell/shrink of clay minerals (Kaiser et al., 2018), or raindrop impact (Hänsel et al., 2016), crusting and degradation of the soil structure are expected due to wetting and drying cycles, causing reduction of soil roughness, or its disturbance by soil animals.

4.2. Evaluation of SfM accuracy

The accuracy of the 3D point coordinates acquired from SfM can be affected by photogrammetric factors such as image geometry and georeferencing (James et al., 2017a). In this study, the spatial variation of LoD was related to the image overlap along the flight. This occurred due to the manual navigation of the UAV used in this study, which required operator care to achieve the necessary coverage of the monitored area. In addition, flight speed must be adjusted to achieve the required overlap among photographs and reduce risks of blurred images at high speeds. Other factors that influence the accuracy of SfM models are surface types (mainly vegetation), soil roughness, and the presence of water (Eltner et al., 2015; James et al., 2017b).

SfM point clouds tend to smooth the soil surface roughness. This can be controlled by the quality parameters in Photoscan during dense cloud generation, but cloud noise might increase when “ultra-high quality” is used (Cook, 2017). Thus, care should be taken when analysing roughness surface data by choosing flight heights, overlap, and image resolution to ensure accurate representation of the soil surface texture at the desired scale. The smoothing of photogrammetric data is well known (Smith et al., 2004; Jester and Klik, 2005); however, the effect of the measurement technique can be considered in combination with the interpolation effect during the generation of DEM or meshing (Lane et al., 2000).

5. Conclusions

This work presents the first evaluation of UAV-SfM for measuring diffuse erosion that has been benchmarked by independent sediment collection data collected from erosion plots under natural rainfall. The high correlation between the soil loss estimated from SfM and collected on erosion plots opens up the possibility to use

SfM for erosion studies where channelized erosion is not the principal mechanism, enabling new insights into diffuse erosion processes.

The use of UAV-based imagery in combination with SfM, represents a low-cost, portable, and easy way to obtain erosion measurements on a smaller scale with high accuracy, in contrast to the traditional standard plot methods of erosion monitoring worldwide. The results of SfM allows not only the quantification of soil loss, for later use in models, but also represents the spatial and temporal dimensions of the soil erosion process, which is of great importance in understanding the mechanisms of the water erosion.

Acknowledgements

The authors would like to thank National Council for Scientific and Technological Development (CNPq, grant numbers 233547/2014-2, 149622/2014-7, 306511/2017-7 and 202938/2018-2), Minas Gerais Research Foundation (FAPEMIG, grant numbers APQ-00802-18 and CAG-APQ 01053-15) and São Paulo Research Foundation (FAPESP, grant number 2018/26366-5) for funding the research on which this study is based.

References

Agüera-Vega F, Carvajal-Ramírez F, Martínez-Carricondo P, López JS, Mesas-Carrascosa FJ, García-Ferrer A, Pérez-Porras FJ. 2018. Reconstruction of extreme topography from UAV structure from motion photogrammetry. Measurement **121**: 127-138.

Al-Hamdan OZ, Pierson FB, Nearing MA, Stone JJ, Williams CJ, Moffet CA, Kormos PR, Boll J, Weltz MA. 2012. Characteristics of concentrated flow hydraulics for rangeland ecosystems: Implications for hydrologic modeling. Earth Surface Processes and Landforms **37**: 157–168.

Araya T, Cornelis WM, Nyssen J, Govaerts B, Bauer H, Gebreegziabher T, Oicha T, Raes D, Sayre KD, Haile M, Decker J. 2011. Effects of conservation agriculture on runoff, soil loss and crop yield under rainfed conditions in Tigray, Northern Ethiopia. Soil Use and Management **27**: 404-414.

Bagarello V, Ferro V. 2004. Plot-scale measurement of soil erosion at the experimental area of Sparacia (southern Italy). Hydrological Processes **18**: 141–157.

Bakker MM, Govers G, Rounsevell MD. 2004. The crop productivity–erosion relationship: an analysis based on experimental work. Catena **57:** 55–76.

Balaguer-Puig M, Marqués-Mateu A, Lerma JL, Ibáñez-Asensio S. 2018. Quantifying small-magnitude soil erosion: Geomorphic change detection at plot scale. Land Degradation & Development **29**: 825–834.

Baumgart P, Eltner A, Domula A, Barkleit A, Faust D. 2017. Scale dependent soil erosion dynamics in a fragile loess landscape. Zeitschrift für Geomorphologie, **61**: 191–206.

Bazoffi P. 2015. Measurement of rill erosion through a new UAV-GIS methodology. Italian Journal of Agronomy **10**: 708.

Boardman J, Evans R, Ford J. 2003. Muddy floods on the South Downs, southern England: problem and responses. Environmental Science & Policy **6**: 69–83.

Castillo C, Pérez R, James MR, Quinton JN, Taguas EV, Gómez JA. 2012. Comparing the accuracy of several field methods for measuring gully erosion. Soil Science Society of America Journal **76**: 1319–1332.

Cerdan O, Govers G, Le Bissonnais Y, Van Oost K, Poesen J, Saby N, Gobin A, Vacca A, Quinton J, Auerswald K, Klik A, Kwaad F, Raclot D, Ionita I, Rejman J, Rousseva S, Muxart T, Roxo M, Dostal T. 2010. Rates and spatial variations of soil erosion in Europe: A study based on erosion plot data. Geomorphology **122**, 167–177.

Cook KL. 2017. An evaluation of the effectiveness of low-cost UAVs and structure from motion for geomorphic change detection. Geomorphology **278**: 195–208.

Colomina I, Molina P. 2014. Unmanned aerial systems for photogrammetry and remote sensing: a review. ISPRS Journal of Photogrammetry and Remote Sensing **92:** 79–97.

Di Stefano C, Ferro V. 2017. Testing sediment connectivity at the experimental SPA2 basin, Sicily (Italy). Land Degradation & Development **28**: 1992–2000.

Di Stefano C, Palmeri V, Pampalone V. 2019. An automatic approach for rill network extraction to measure rill erosion by terrestrial and low-cost unmanned aerial vehicle photogrammetry. Hydrological Processes **33**: 1883–1895.

Dietrich JT. 2016. Riverscape mapping with helicopter-based Structure-from-Motion photogrammetry. Geomorphology **252**: 144–157.

Easa SM. 1988. Estimating pit excavation volume using nonlinear ground profile. Journal of Surveying Engineering **114**: 71–83.

Eltner A, Baumgart P, Maas HG, Faust D. 2015. Multi-temporal UAV data for automatic measurement of rill and interrill erosion on loess soil. Earth Surface Processes and Landforms **40**: 741–755.

Eltner A, Maas H-G, Faust D. 2018. Soil micro-topography change detection at hillslopes in fragile Mediterranean landscapes. Geoderma **313:** 217–232.

Fang NF, Wang L, Shi ZH. 2017. Runoff and soil erosion of field plots in a subtropical mountainous region of China. Journal of Hydrology **552:** 387–395.

Fawzy HE. 2015. The accuracy of determining the volumes using close range photogrammetry. IOSR Journal of Mechanical and Civil Engineering **12**: 10–15.

Fonstad MA, Dietrich JT, Courville BC, Jensen JL, Carbonneau PE. 2013. Topographic structure from motion: a new development in photogrammetric measurement. Earth Surface Processes and Landforms **38**: 421–430.

García-Ruiz JM, Beguería S, Nadal-Romero E, González-Hidalgo JC, Lana-Renault N, Sanjuán Y. A meta-analysis of soil erosion rates across the world. Geomorphology **239**: 160–173.

Gelman A, Hill J. 2007. Data analysis using regression and multilevel/hierarchical models. Cambridge University Press, New York.

Gómez-Gutiérrez A, Schnabel S, Berenguer-Sempere F. 2014. Using 3D photo-reconstruction methods to estimate gully headcut erosion. Catena **120**: 91–101.

Glendell M, McShane G, Farrow L, James M, Quinton J, Anderson K, Evans M, Benaud P, Rawlins B, Morgan D, Jones L, Kirkham M, DeBell L, Quine T, Lark M, Rickson J, Brazier R. 2017. Testing the utility of structure from motion photogrammetry reconstructions using small unmanned aerial vehicles and ground photography to estimate the extent of upland soil erosion. Earth Surface Processes and Landforms **42**: 1860–1871.

Guo M, Shi H, Zhao J, Liu P, Welbourne D, Lin Q. 2016. Digital close range photogrammetry for the study of rill development at flume scale. Catena **143**: 265–274.

Guo Q, Hao Y, Liu B. 2015. Rates of soil erosion in China: a study based on runoff plot data. Catena **124**: 68–76.

Hänsel P, Schindewolf M, Eltner A, Kaiser A, Schmidt J. 2016. Feasibility of high-resolution soil erosion measurements by means of rainfall simulations and SfM photogrammetry. Hydrology **3**: 38.

Hernandez M, Nearing MA, Al-Hamdan OZ, Pierson FB, Armendariz G, Weltz MA, Spaeth KE, Williams CJ, Nouwakpo SK, Goodrich DC, Unkrich CL, Nichols MH, Collins CDH. 2017. The Rangeland Hydrology and Erosion Model: A Dynamic Approach for Predicting Soil Loss on Rangelands. Water Resources Research **53**: 9368–9391.

James MR, Robson S. 2012. Straightforward reconstruction of 3D surfaces and topography with a camera: accuracy and geoscience application. Journal of Geophysical Research **117**: F03017.

James MR, Robson S. 2014. Mitigating systematic error in topographic models derived from UAV and ground-based image networks. Earth Surface Processes and Landforms **39**: 1413–1420.

James MR, Robson S, Smith MW. 2017a. 3-D uncertainty-based topographic change detection with structure-from-motion photogrammetry: precision maps for ground control and directly georeferenced surveys. Earth Surface Processes and Landforms **42**: 1769–1788.

James MR, Robson S, d'Oleire-Oltmanns S, Niethammer U. 2017b. Optimising UAV topographic surveys processed with structure-from-motion: Ground control quality, quantity and bundle adjustment. Geomorphology **280**: 51–66.

Jester W, Klik A. 2005. Soil surface roughness measurement—methods, applicability, and surface representation. Catena **64**: 174–192.

Kaiser A, Erhard A, Eltner A. 2018. Addressing uncertainties in interpreting soil surface changes by multi-temporal high resolution topography data across scales. Land Degradation & Development **9**: 2264–2277.

Kou P, Xu Q, Yunus AP, Ju Y, Guo C, Wang C, Zhao K. 2019. Multi-temporal UAV data for assessing rapid rill erosion in typical gully heads on the largest tableland of the Loess Plateau, China. Bulletin of Engineering Geology and the Environment.

Lal R. 1998. Soil erosion impact on agronomic productivity and environment quality. CRC Critical Reviews in Plant Sciences **17**: 319–464.

Lane SN, James TD, Crowell MD. 2000. Application of digital photogrammetry to complex topography for geomorphological research. Photogrammetric Record **16**: 793–821.

Lane SN, Westaway RM, Hicks DM. 2003. Estimation of erosion and deposition volumes in a large, gravel-bed, braided river using synoptic remote sensing. Earth Surface Processes and Landforms **28**: 249–271.

Morgan RPC. 2005. Soil Erosion and Conservation. third ed. Blackwell Publishing Ltd., Cornwall.

Morgan JA, Brogan DJ, Nelson, PA. 2017. Application of Structure-from-Motion photogrammetry in laboratory flume. Geomorphology **276**, 125–143.

Neugirg F, Stark M, Kaiser A, Vlacilova M, Della Seta M, Vergari F, Schmidt J, Becht M, Haas F. 2016. Erosion processes in calanchi in the upper Orcia Valley, southern Tuscany, Italy based on multitemporal high-resolution terrestrial LiDAR and UAV surveys. Geomorphology **269:** 8–22.

Nouwakpo S, Weltz M, McGwire K. 2015. Assessing the performance of structure-from-motion photogrammetry and terrestrial lidar for reconstructing soil surface microtopography of naturally vegetated plots. Earth Surface Processes and Landforms **41**: 308–322.

Nouwakpo SK, Williams CJ, Al-Hamdan OZ, Weltz MA, Pierson F, Nearing M. 2016. A review of concentrated flow erosion processes on rangelands: Fundamental understanding and knowledge gaps. International Soil and Water Conservation Research **4**: 75–86.

Papiernick SK, Schumacher TE, Lobb DA, Lindstrom MJ, Lieser ML, Eynard A, Schumacher JA. 2009. Soil properties and productivity as affected by topsoil movement within an eroded landform. Soil & Tillage Research **102**: 67–77.

Parsons AJ. 2019. How reliable are our methods for estimating soil erosion by water?. Science of the Total Environment **676**: 215–221.

Phan Ha HAP, Huon S, Henry des Tureaux TH, Orange D, Jouquet P, Valentin C, De Rouw A, Tran Duc TT. 2012. Impact of fodder cover on runoff and soil erosion at plot scale in a cultivated catchment of North Vietnam. Geoderma **177**: 8–17.

Pineux N, Lisein J, Swerts G, Bielders CL, Lejeune P, Colinet G, Degré A. 2017. Can DEM time series produced by UAV be used to quantify diffuse erosion in an agricultural watershed?. Geomorphology **280**: 122–136.

Quinton JN, Govers G, Van Oost K, Bardgett RD. 2010. The impact of agricultural soil erosion on biogeochemical cycling-s2. Nature Geoscience **3**: 1–6.

Seitz SM, Curless B, Diebel J, Scharstein D, Szeliski R. 2006. A comparison and evaluation of multi-view stereo reconstruction algorithms. IEEE Conference on Computer Vision and Pattern Recognition. IEEE Computer Society, New York.

Smith MJ, Asal FFF, Priestnall G. 2004. The use of photogrammetry and lidar for landscape roughness estimation in hydrodynamic studies. International Archives of the Photogrammetry, Remote Sensing and Spatial Information Sciences **35**: 714–719.

Soil Survey Staff, 1999. Soil taxonomy: a basic system of soil classification for making and interpreting soil surveys, Agricultural Handbook 436, 2nd edition. Natural Resources Conservation Service, USDA, Washington D.C.

Stöcker C, Eltner A, Karrasch P. 2015. Measuring gullies by synergetic application of UAV and close range photogrammetry — a case study from Andalusia, Spain. Catena **132**: 1–11.

Taylor JR. 1997. An Introduction to Error Analysis: the Study of Uncertainties in Physical Measurements, second edition. University Science Books: Sausalito, California.

Ullman S. 1979. The interpretation of structure from motion. Proceedings of the Royal Society of London. Series B, Biological Sciences **203**: 405–426.

Warrick J, Ritchie A, Adelman G, Adelman K, Limber P. 2017. New techniques to measure cliff change from historical oblique aerial photographs and structure-from-motion photogrammetry. Journal of Coastal Research **33**: 39–55.

Westoby M, Brasington J, Glasser N, Hambrey M, Reynolds J. 2012. ‘Structure- from-motion’ photogrammetry: a low-cost, effective tool for geoscience applications. Geomorphology **179**: 300–314.

Westoby M, Dunning S, Woodward J, Hein A, Marrero S, Winter K, Sugden D. 2016. Interannual surface evolution of an Antarctic blue-ice moraine using multi-temporal DEMs. Earth Surface Processes and Landforms **4**: 515–529.

Wheaton J, Brasington J, Darby S, Sear D. 2010. Accounting for uncertainty in DEMs from repeat topographic surveys: improved sediment budgets. Earth Surface Processes and Landforms **35**: 136–156.

Zhao J, Van Oost K, Chen L, Govers G. 2016. Moderate topsoil erosion rates constrain the magnitude of the erosion-induced carbon sink and agricultural productivity losses on the Chinese Loess Plateau. Biogeosciences **13**: 4735–4750.

Zhao J, Yang Z, Govers G. Soil and water conservation measures reduce soil and water losses in China but not down to background levels: Evidence from erosion plot data. Geoderma **337**: 729–741.

Zobisch MA, Klingspor P, Oduor AR. 1996. The accuracy of manual runoff and sediment sampling from erosion plots. Journal of Soil and Water Conservation **51**: 231–1233.

Zuur AF, Ieno EN, Walker NJ, Saveliev AA, Smith GM. 2009. Mixed effects models and extensions in ecology with R. Springer, New York, New York, USA.